Received: 4 March 2021 | Revised: 19 April 2021 | Accepted: 22 April 2021

DOI: 10.1002/er.6888

RESEARCH ARTICLE

INTERNATIONAL JOURNAL OF ENERGY RESEARCH WILEY

A new solar atmospheric water harvesting integrated system using CPV/T – Stirling engine – Absorption cooling cycle and vapor compression refrigeration cycle

Ibrahim Al Keyyam | **Moh'd Al-Nimr** | **Saud Khashan** | **Ashraf Keewan**

Department of Mechanical Engineering, Jordan University of Science and Technology, Irbid, Jordan

Correspondence
Ibrahim Al Keyyam, Department of Mechanical Engineering, Jordan University of Science and Technology, P.O.Box 3030, Irbid 22110, Jordan.
Email: ioalkeyyam17@eng.just.edu.jo

Summary

This research theoretically investigates the performance of a new integrated solar atmospheric water harvesting system. The system consists of a concentrated photovoltaic thermal unit (CPV/T) to capture solar radiation and produce electricity. The rejected heat is utilized to drive an alpha-type Stirling engine and a single effect $LiBr/H_2O$ absorption cooling cycle (ACC). The power output of the Stirling engine and the CPV/T is used to drive a vapor compression refrigeration cycle (VCRC), whereas the cooling capacity of the cooling cycles is used to cool and dehumidify ambient air and generate potable water. Moreover, a heat recovery heat exchanger is employed to pre-cool the supply air before entering the evaporator, thus increasing the water production rate. The model is validated and solved numerically. A parametric study is conducted to show the effect of a variety of ambient and operating conditions on the system's performance. The highest water production rate is found, as expected, to be in hot and humid climates where the solar radiation, the ambient temperature, and the relative humidity are high. The freshwater production exhibits a non-monotonic behavior with increasing the air mass flow rate, and the maximum potable water production was identified. At solar radiation values of 0.6, 0.8, and 1 (kW/m^2), the maximum water production was generated at air mass flow rate values of 1.6, 2.8, and 3.8 (kg/s), and the corresponding maximum water production were 13.37, 20.12, and 26.28 (L/h), respectively. It is found that this integrated system can produce up to 30 L/h under hot and humid ambient conditions, and pre-cooling of the supplied air yields better performance under drier conditions. The proposed system is suitable for small-scale applications where water demand is less than 180 L/day. It is found that the amount of electrical energy consumed per liter of produced water by this system is between 225 and 315 Wh/L approximately.

KEYWORDS

absorption cooling cycle, atmospheric water harvesting, CPV/T, solar thermal utilization, Stirling engine

Abbreviations: ACC, Absorption cooling cycle; COP, Coefficient of performance; CPV/T, Concentrated photovoltaic thermal; EES, Engineering equations solver; HX, Heat exchanger; LMTD, Log mean temperature difference (°C); SE, Stirling engine; VCRC, Vapor compression refrigeration cycle.

1 | INTRODUCTION

Freshwater is vital to human survival and economic development. The amount of fresh water on land accounts only for 2.53% of all water on the planet, much of it takes the forms of glaciers and deep groundwater which makes it difficult to exploit.[1] Only 0.26% of the total worldwide water reserves (90 000 km^3) is accessible for human use from rivers, lakes, and shallow groundwater. Furthermore, the increased human populations and their emission-producing activities continuously limiting these freshwater resources.[1] Water shortage is deemed to cause one of the most daunting problems for humanity in the future. At the slightest, 3.3 billion individuals around the world encounter water shortage, an issue that is expanding with the potential of causing more clashes between nations competing for a continuously depleting asset.[2] The depletion of freshwater resources, compounded with the unfavorable shifts in the rainfall patterns caused by climate change, poses a great challenge that requires urgent handling. Numerous strategies have been utilized to collect water such as water desalination, groundwater gathering, and rainwater collection. For these strategies to work, water must be accessible, but when such supplies are restricted, atmospheric water harvesting gets to be crucial. Hence, not surprisingly, it is now earning huge consideration from researchers all around the world.

The atmosphere is a massive water reservoir enclosing the Globe. It is estimated that the atmosphere holds a total of over 12.9×10^{12} m^3 of renewable water.[3] In wetlands, this amount gets even greater than that of the conventional sources of freshwater. The extraction of fresh water from the atmosphere becomes an even more viable option in remote areas. The production of water from ambient air is regarded as a source of renewable water. The technical feasibility of the process, particularly near tropical and coastal areas where temperature and humidity levels are typically high, was proved evident in most of the research works. However, this technical feasibility was generally attained via energy-intensive systems.

In general, extracting water from atmospheric air can be achieved using one of two main techniques; cooling surfaces and sorption cycles. In the sorption technique, distinctive solvents or sold mediums are used to captivate water molecules and, then, re-desorbe them by heating. While in the first technique, the temperature of humid air, when put into contact with the cooling surfaces, is decreased below the dew point. The cooling of these surfaces requires a high-energy process. In many cases, such high energy consumption can be justified if it is used to serve both cooling and water production at the same time. Cooling surfaces can be achieved, among other means, using refrigeration cycle systems. For example, modified air conditioners were used to harvest water from the air.[4,5] An analytical and experimental study was done on a 1.5-ton split unit during humid and hot summer months.[6] The results indicate that the air temperature and its humidity ratio at the inlet and the outlet are the main factors affecting water productivity. Also, the study reported that the produced water requires microbial treatment before it could be consumed by humans. The absorption cycle is another refrigeration system used for water harvesting. Solar vapor absorption was used to extract water from fresh air.[7] An evacuated tube solar collector was used to drive the absorption cycle's generator. The results indicate that the increase in the solar radiation intensity enhances the absorption cycle COP, the efficiency of the collector, and the water production of the system. Salek et al[8] studied a system driven by a solar-driven ammonia absorption cycle. The proposed system produces water using both dehumidification and desalination subsystems. An absorption chiller is used to provide for the dehumidification while its waste heat is used to heat the saline water introduced to the desalination system. They reported an improvement of 165% in comparison with the common atmospheric water generator. Magrini et al[9] studied the feasibility of water production using the condensation by chillers used for cooling a hotel with a cooling capacity of 3600 kW. The study estimated a water production of up to 10 (m^3/day) during July through September.

An alternative for the conventional refrigeration systems, thermo-electrical cooler systems (TECS) is used to serve the cooling surfaces technique.[10-15] Eslami et al[14] used 15-20 TECS to extract water from atmospheric air. A PV system was used to power the TECS and a supply fan was added for the air circulation process. Optimal water production per energy consumed unit was reported. Only 20 W of electrical power was sufficient to harvest 26 mL/h from the ambient air stream with 318 K and 75% relative humidity. Joshi et al[10] presented a portable atmospheric water harvesting device, proposed for coastal and humid regions, using TECS. Adding heat sink at the cold side of the TEC module enhanced the heat transfer, and therefore, the water production by 81%. Milani et al[11] conducted a parametric and economical study of another system using TECS integrated with a rainwater harvesting system. The amount of the harvested water and the energy demand was determined using correlated psychometric variables. The results show that the energy cost accounted for 95% of the total cost.

Indeed, water and energy global challenges are two sides of the same coin. Most water treatment techniques

need energy. In other words, the high energy demand has posed the greatest challenge for water treatment processes and has been the main concern driving more developments. Renewable energy is the most promising alternative source to cut on the high energy demand needed for water harvesting systems. Different renewable energy systems are used to drive these systems such as photovoltaic systems (PV), concentrated photovoltaic thermal systems (CPVT), wind energy systems, and Stirling engine systems. Furthermore, the water harvesting systems can be driven by electrical energy produced from a renewable source or by recovering waste energies. Giwa et al[16] proposed driving a humidification–dehumidification water production system by the waste heat of PV panels and which is reported capable of producing an average daily production of 2.28 L/m^2 under UAE climate conditions. Mahmoud et al[17] combined thermally cooled PV panels and a solar concentrator with a hybrid humidification–dehumidification/solar still system. In addition to generating electricity, the PVT panels were used for preheating water before feeding the humidifier. Adding PVT system contributed to enhancement in water production that is found to be directly proportional to the solar concentration ratio. Jabari et al[18] presented a renewable energy system to cover the energy and water demands of a hotel building in Iran. The proposed system consisted of a solar dish, a Stirling engine, a humidification–dehumidification desalination system, and an air conditioning system. The waste heat of the Stirling engine was utilized to drive the desalination system and its electrical power output was used to drive the hotel air conditioning system. Al Nimer and Ammari[19] introduced a hybrid solar system that uses a solar-driven Stirling engine to drive a TECs and water desalination unit to produce electricity and to harvest water. In their system, desalination still water is cooled by the TECs' cold side and preheated by the waste of the Stirling engine cold side and the TECs' hot side. They reported that coupling the desalination still with TEC and SE systems increases its productivity rate from 2.93 to 40.96 kg/s.

Recently, many researchers were proposed different systems to enhance the efficiency of the atmospheric water harvesting process. Elashmawy and Alshammari[20] proposed using tubular solar still for AWH for arid regions. A parabolic concentrator system was used to activate the solar still to enhance its ability to evaporate water under low humid conditions. The study was done based on the climate conditions of Hali city in Saudi Arabia. It was found that the new system has 24.61% thermal efficiency which was 82.3% more than the stand-alone tubular solar still. Also, using the parabolic concentrator system enhanced productivity by 292.4% and reduce the water production cost by 25%. A new device that works based on adsorption phenomena was proposed by Wang et al[21] for atmospheric water harvesting. The most attractive feature of using the adsorption base water harvesting method is its efficiency and applicability even in low relative humidity areas. The device was fabricated from ACFF-Silica sol-LiCl. The results showed that the system had 0.37 thermal efficiency and 7.7 kg of water per day and night cycle. The device was suggested to be used in the island regions which have a shortage of drinking water.

Al-Nimr et al[22] have proposed a novel approach to improve the performance of a solar-driven Stirling engine; by using a solar-driven ejector cooling cycle. The cooling effect of the ejector will be used, partially or totally, in cooling the cold side of the Stirling engine to improve its efficiency and produce more electric power. The core objective of their research was to check the feasibility of splitting the collected thermal energy into two parts. This is in order to check if sacrificing part of the thermal energy to cool the cold side of the engine, via the ejector, is better than utilizing all thermal energy in heating the hot side of the engine. The first part of the thermal energy was used to drive the Stirling engine, and the second part to drive the ejector cooling system. Besides, the rejected heat from the ejector cooling cycle may be utilized in preheating the hot fluid that drives the Stirling engine before returning to the solar concentrator. By implementing this novel integration, it is found that the Stirling engine will generate more electricity from the same incident solar radiation, which implies a significant improvement in the system efficiency. This is, of course, in addition to the ability of the system in generating both electricity, heating, and cooling effects. The authors also have studied the effect of different design and operating parameters on the integrated system performance. Examples are in using variable working fluid rates through the cooling ejector.

Based on our survey concerning the literature about atmospheric water harvesting systems, all the previous papers have used either electrical or thermal power to drive the harvesting process. As a result, this paper's unique contribution is to merge the two; by using the rejected thermal energy from electrical power systems to drive a heat-driven cooling cycle, thus increasing the system's cooling effect. Besides, no research work is identified to investigate the prospect of integrating the CPV/T, Stirling, absorption cooling cycle (ACC), and the refrigeration cooling cycle for the production water from atmospheric air. This paper proposes a new integrated system that produces freshwater, cooling, heating, and electrical power, where the main objective is to provide fresh water in water-scarce areas. The system's steady-state operation is investigated and evaluated under various operating

and design parameters (solar radiation, outside air temperature, outside air relative humidity, and outside air mass flow rate). Engineering Equation Solver (EES) software is used to develop and solve the mathematical model of the systems numerically. The influence of various design and operating parameters on the system's performance (freshwater production rate, system electrical power output, system cooling capacity, and system coefficient of performance) are studied. For evaluation and assessment of the proposed system, comparisons with other technologies and previous studies have been done.

2 | MODEL DESCRIPTIONS AND VALIDATION

This research proposed a new atmospheric water harvesting integrated system, which consists of four main parts: (a) concentrated photovoltaic thermal unit (CPV/T); (b) alpha-type Stirling engine system with a finite shaft rotating speed (SE); (c) single effect LiBr/H_2O ACC; and (d) vapor compression refrigeration cycle (VCRC). The components of the proposed system are interacting in a way that enhances the performance of each component. The CPV/T utilizes solar energy to produce electricity and thermal energy stored in water as the working fluid. Cooling the photovoltaic panels is mandatory under concentration, and it yields in enhancing their efficiency. The rejected thermal energy is utilized in driving the Stirling engine, which is known for its high efficiency that is ideally equal to that of Carnot. Moreover, the remainder thermal energy is utilized in driving an ACC, which is normally driven by low-grade heat. This would increase the cooling effect for the harvesting process and simultaneously decrease the inlet temperature for the CPV/T. The electrical power produced by the Stirling engine and the CPV/T would run a vapor compression cycle. The cooling power of the ACC and the VCRC is used to cool and dehumidify ambient air and produce water. To enhance the water production rate, a heat recovery heat exchanger is employed at the air inlet to pre-cool the supplied air, thus reduces the required sensible cooling for the condensation to start.

2.1 | Concentrated photovoltaic thermal system

To simplify the model, the following assumptions are considered:

1. The system operates in steady-state conditions.
2. The conductive thermal resistance through the glass cover and the photovoltaic layer can be negligible.
3. The absorptivity of the glass can be neglected.

The amount of electrical power produced by the photovoltaic cell (P_{PV}) is given as Reference 23:

$$P_{PV} = I\,A_c\,\lambda\,\tau_g(\tau\alpha)_{PV}\eta_{PV} \tag{1}$$

where I is the solar radiation intensity, A_c is the aperture area, λ is mirror utilization factor, τ_g is the transmissivity of glass, $(\tau\alpha)_{PV}$ is the absorptivity and transmissivity product of the photovoltaic cells, and η_{PV} is the efficiency of the photovoltaic panel which is calculated as Reference 24:

$$\eta_{PV} = \eta_0\,(1-\beta_{ref}\,(T_{PV}-T_{ref})) \tag{2}$$

where η_0 is the photovoltaic cells' efficiency at standard conditions, β_{ref} is the temperature coefficient (K^{-1}) at 25°C, T_{PV} is the photovoltaic cell temperature, and T_{ref} is the reference temperature at standard conditions.

The majority of the solar radiation is stored as thermal energy and stored in the working fluid. The useful thermal energy absorbed by the water is calculated as Reference 25:

$$Qu = FR\big((I\,A_c\,\lambda)\,\tau_g\,(\tau\alpha)_{PV}(1-\eta_{PV}) - A_{pv}U_L(T_1-T_a)\big) \tag{3}$$

$$Qu = \dot{m}\,C_p\,(T_2-T_1) \tag{4}$$

where A_{PV} is the photovoltaic panel area and T_1, and T_a are the CPV/T fluid inlet temperature, and ambient air temperature, respectively. The heat removal factor FR can be calculated as Reference 25:

$$FR = \frac{\dot{m}\,C_p}{A_{pv}\,U_L}\left[1-\exp\left(-\frac{U_L A_{pv}\,F'}{\dot{m}\,C_p}\right)\right] \tag{5}$$

where F' is the collector efficiency factor, and it is calculated as Reference 25:

$$F' = \frac{\frac{1}{U_L}}{\frac{1}{U_L}+\frac{D_o}{h_{fi}\,D_i}+\left(\frac{D_o}{2\,K_c}\ln\left(\frac{D_o}{D_i}\right)\right)} \tag{6}$$

where D_i is the tube's inner diameter and D_o is the tube's outer diameter. U_L represents the overall heat loss coefficient and it is given as Reference 25:

$$U_L = \left(\frac{A_{PV}}{(h_w + \boldsymbol{h_{r\,a-g}})\,Ag} + \frac{1}{\boldsymbol{h_{r\,g-pv}}} \right)^{-1} \tag{7}$$

where A_g is the area of the glass cover, $h_{r\,g-pv}$ and $h_{r\,a-g}$ are the radiative heat transfer coefficients from the photovoltaic panel to the glass layer and from the glass layer to the ambient air, respectively. They are determined as Reference 26:

$$h_{r\,a-g} = \sigma\,\varepsilon\,(T_g + T_{sky})\,(T_g{}^2 + T_{sky}{}^2) \tag{8}$$

$$h_{r\,g-pv} = \sigma\,\frac{(T_g + T_{pv})\,(T_g{}^2 + T_{pv}{}^2)}{\frac{1}{\varepsilon_{pv}} + \frac{D_{pv}}{D_g}\left(\frac{1}{\varepsilon_g} - 1\right)} \tag{9}$$

where ε_g is the glass layer emissivity, ε_{pv} is the photovoltaic panel emissivity, $T_g$is the temperature of the glass cover, and T_{Sky} is sky temperature which can be calculated by Reference 27:

$$T_{Sky} = 0.0552\,T_a{}^{1.5} \tag{10}$$

Going back to Equation (7), h_w represents the convective heat transfer coefficient outside the glass layer, which is calculated as Reference 26:

$$h_w = \frac{Nu\,K_a}{D_g} \tag{11}$$

where D_g is the glass cover diameter, K_a is the air conductivity, and Nu is the Nusselt number which is estimated using the following correlation[25]:

$$Nu = 0.3 + \frac{0.62\,Re^{1/2}\,Pr^{1/3}}{\left(1 + \left(\frac{0.4}{Pr}\right)^{\frac{2}{3}}\right)^{1/4}} \left(1 + \left(\frac{Re}{282000}\right)^{\frac{5}{8}}\right)^{4/5} \tag{12}$$

where Pr is Prandtl number and Re is Reynold number and is calculated as Reference 26:

$$Re = \frac{\rho\,V\,D_g}{\mu} \tag{13}$$

To calculate the collector efficiency factor in Equation (6), h_{fi} represents the convection heat transfer coefficient inside the copper tube. It must be known first and is calculated by Reference 26:

$$Nu = \frac{\left(\frac{f}{8}\right)(Re - 1000)\,Pr}{1 + 12.7\left(\frac{f}{8}\right)^{0.5}\left(Pr^{\frac{2}{3}} - 1\right)} \tag{14}$$

$$\frac{1}{\sqrt{f}} = -2.0\,Log\left(\frac{\frac{\in}{D_i}}{3.7} + \frac{2.51}{Re\sqrt{f}}\right) \tag{15}$$

$$h_{fi} = \frac{K_w}{D_i}\,Nu \tag{16}$$

where K_w is the conductivity of water, f represents the friction factor, and $\in$ is the surface roughness.

2.2 | Stirling engine system

For simplicity, the following assumptions are considered:

1. The system operates at steady-state conditions.
2. Heat leakage is neglected; therefore, the supplied heat is absorbed completely by the hot gas.
3. Heat is added to and rejected from the engine isothermally.

According to the assumptions, the required heat from an external source for the engine to operate at a constant frequency must equal the heat supplied by the hot oil stream and must be equal to the heat transferred through the heat exchanger into the hot cylinder.

The heat supplied by the hot oil stream takes the form:

$$Q_H = \dot{m}_c C_p (T_2 - T_3) \tag{17}$$

where T_2 is the heater heat exchanger inlet oil temperature which equals the solar collector outlet temperature and T_3 is the heater heat exchanger outlet temperature as shown in Figure 1.

For an isothermal Stirling engine model, the heat addition is assumed to occur at a constant temperature of charged gas T_H. During the heating process as the hot oil temperature varies, the heat transferred in the heater can be calculated as Equation (18)[28,29]:

$$Q_H = K_H \frac{(T_2 - T_H) - (T_3 - T_H)}{Ln\left(\frac{(T_2 - T_H)}{(T_3 - T_H)}\right)} \tag{18}$$

where T_H is the gas temperature at the hot end and K_H heat transfer's ability of the heater heat exchanger which is calculated as:

$$K_H = h_H A_{s,H} \tag{19}$$

where $A_{s,H}$ is the heater surface area.

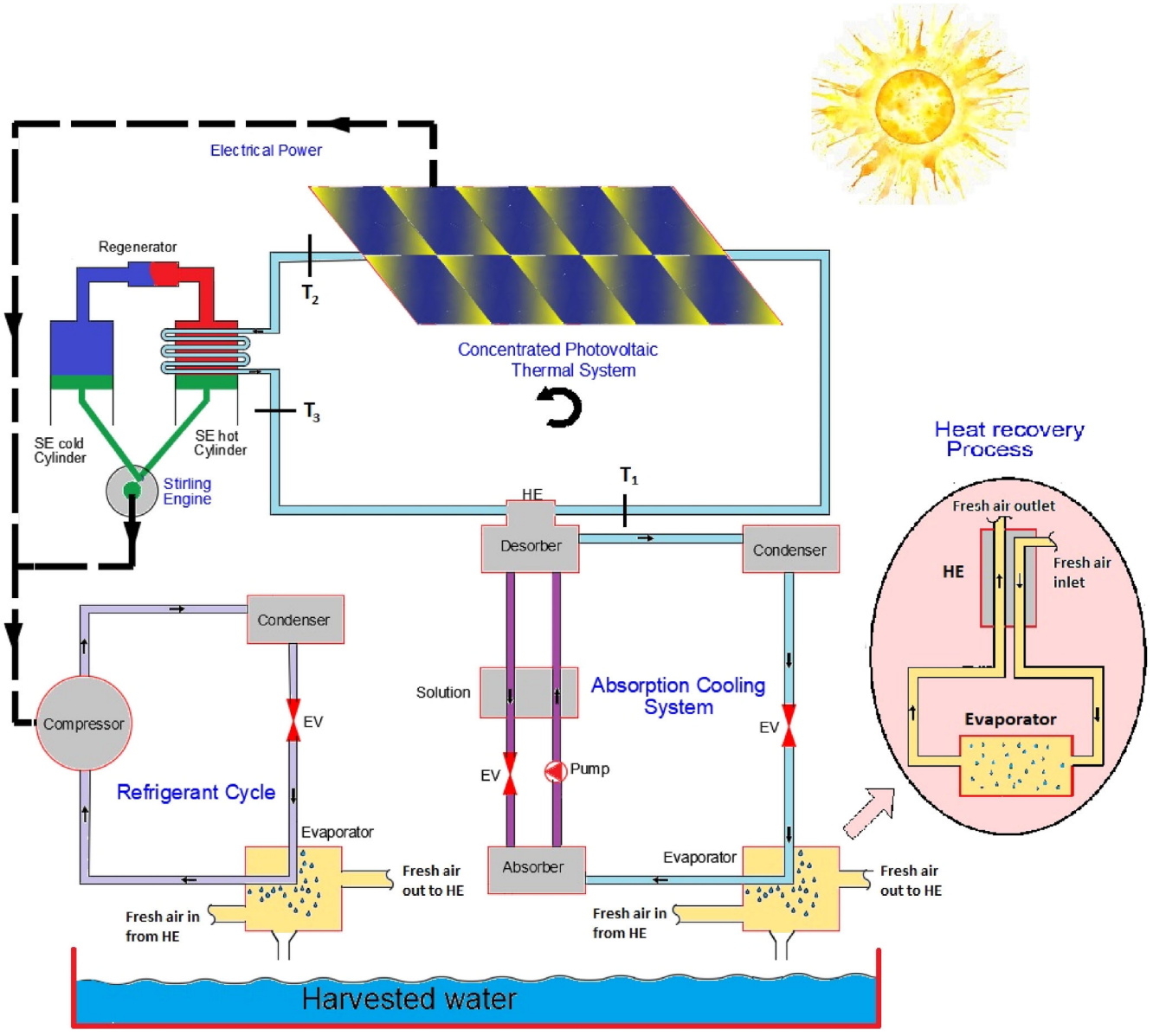

FIGURE 1 Proposed system model [Colour figure can be viewed at wileyonlinelibrary.com]

Heat requirement rate from external heat source for the engine to rotate at constant speed is given as Reference 30:

$$Q_H = Fm_{He}C_v(T_H - T_L)(1-\varepsilon_R) + Fm_{He}R_g(T_H+273)Ln\left(\frac{v_4}{v_3}\right) \quad (20)$$

where F is the frequency of rotating shaft, C_v is the specific heat at constant volume for charged gas, ε_R is the effectiveness of the regenerator, m_{He} is the helium mass inside the cylinder, R_g is the gas constant for helium, and v is the specific volume of helium.

The required heat to be extracted from the charged gas for the cycle to operate is calculated as Reference 30:

$$Q_L = Fm_{He}C_v(T_H - T_L)(1-\varepsilon_R) - Fm_{He}R_g(T_L+273)Ln\left(\frac{v_1}{v_2}\right) \quad (21)$$

The extracted heat by the ambient air is given by:

$$Q_L = h_{conv}A_{s,L}\varepsilon_{fin}(T_L - T_a) \quad (22)$$

where h_{conv} is the convective heat transfer coefficient, $A_{s,L}$ is the cooler area, ε_{fin} is the effectiveness of the fins, and T_L is the heat rejection temperature.

The output power produced by the engine is calculated as:

$$P_{SE} = F m_{He} R_g (T_H - T_L) Ln\left(\frac{v_1}{v_2}\right) \quad (23)$$

The efficiency of the engine is given as:

$$\eta_{SE} = \frac{P_{SE}}{Q_H} \quad (24)$$

2.3 | Absorption cooling cycle

To simplify the analysis, the following assumptions are considered:

1. The vapor at the desorber's outlet is pure refrigerant.
2. The refrigerant leaves the evaporator and the condenser as saturated.
3. The pumping process is isentropic.

The model is constructed by applying the conservation of energy and mass principles for each part of the cycle as References 31,32:

$$\sum \dot{m}_i = \sum \dot{m}_o \quad (25)$$

$$\sum \dot{m}_i X_i = \sum \dot{m}_o X_o \quad (26)$$

$$\sum \dot{m}_i h_i - \sum \dot{m}_o h_o = W - Q \quad (27)$$

For each heat exchanger, the heat transfer rate (Q) is calculated as Reference 31:

$$Q = (UA)(LMTD) \quad (28)$$

where the overall coefficient of heat transfer multiplied by the area is UA, and the log mean temperature differential is $LMTD$.

The coefficient of performance of the absorption cycle is calculated as Reference 31:

$$COP_{ACC} = \frac{Q_{e,ACC}}{Q_d} \quad (29)$$

2.4 | Vapor compression cycle

The COP of the vapor compression cycle is assumed to be 3.5 as the highest possible practical COP in literature.[33] The electrical power output of the Stirling engine and the concentrated photovoltaic cells is used to drive the compressor, and the output cooling power is given as:

$$Q_{e,VCRC} = (COP_{VCRC})(P_{tot}) \quad (30)$$

2.5 | Cooling and dehumidification system

The dehumidification process is modeled as in Reference 34, where the energy balance is given by:

$$Qe = \dot{m}_{air}(h_{air,i} - h_{air,o}) - \dot{m}_{water} h_{water} \quad (31)$$

where Qe is the evaporator cooling power, $h_{air,i}$ is the enthalpy of air at the inlet, $h_{air,o}$ is the enthalpy of the air at the outlet of the evaporator, $\dot{m}_{water}$ is the harvested water mass flow rate, and h_{water} is the enthalpy of harvested water.

The mass balance for water vapor is given as:

$$\dot{m}_{water} = \dot{m}_{air}(\omega_i - \omega_o) \quad (32)$$

where ω_i and ω_o are the specific humidity ratio of the air at the inlet and the outlet, respectively.

The effectiveness of the heat recovery heat exchanger is given by Reference 35:

$$\epsilon_{hr,HX} = \frac{(h_{amb} - h_{air,i})}{(h_{amb} - h_{air,o})} \quad (33)$$

where h_{amb} is the enthalpy of supplied air at ambient conditions.

The recovered heat by the heat exchanger is given by Reference 26:

$$Q_{recovered} = \dot{m}_{air}(h_{amb} - h_{air,i}) \quad (34)$$

2.6 | Model validation

The current model of the Stirling engine used in this research was conducted based on the model proposed by Lai et al[30] where a modified mathematical model for a constant speed alpha type Stirling engine driven by a solar dish that transfers the solar thermal radiation to the charged gas through a receiver. The proposed model in our research is modified to be driven by a CPV/T that uses water as the working fluid and transfers the thermal energy to charged gas through a heat exchanger rather than a solar dish. The results of the current model of the Stirling engine were compared to the theoretical reported by Reference 30 under the same conditions and showed a good agreement as shown in Figure 2. As for the ACC, the model proposed by Herold and Klein[31] was simulated using the current model, and Table 1 presents the input parameters taken from Reference 31 for validation. The results of the current model of the absorption cooling system were compared to that reported in Reference 31 and

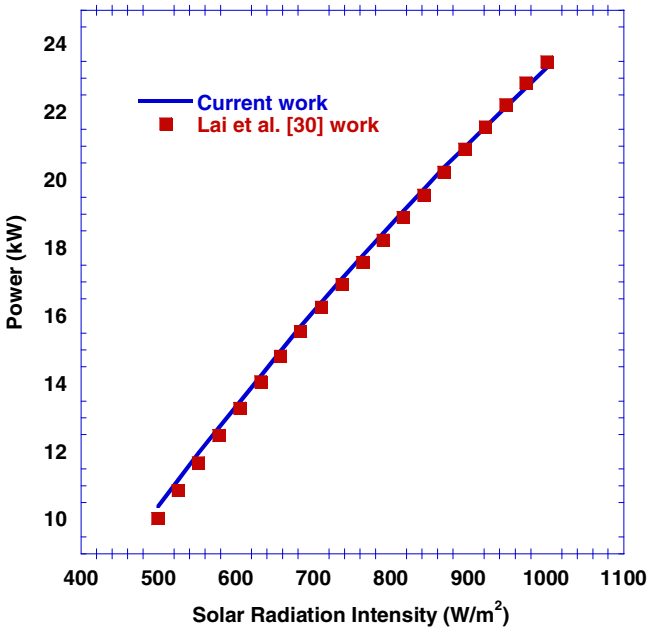

FIGURE 2 Stirling engine system validation [Colour figure can be viewed at wileyonlinelibrary.com]

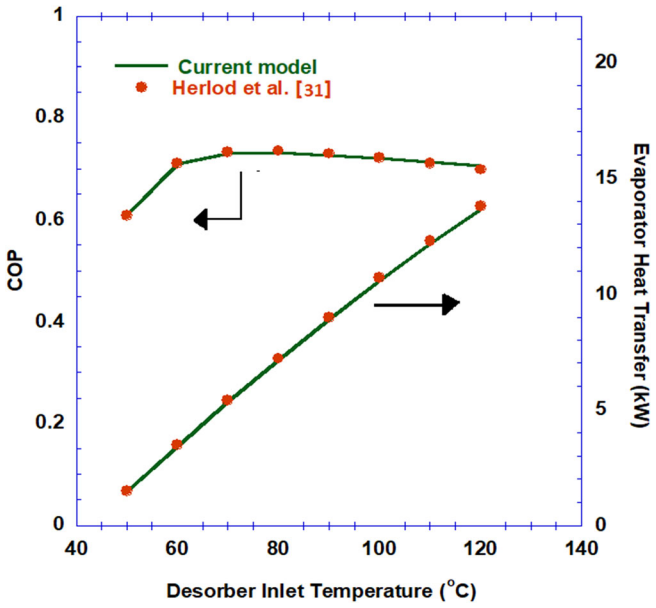

FIGURE 3 Absorption cooling system validation [Colour figure can be viewed at wileyonlinelibrary.com]

TABLE 1 Absorption cooling cycle (ACC) simulation parameters used by Reference 31

Parameter	Value
UA_a	1.8 (kW/°C)
UA_c	1.2 (kW/°C)
UA_d	1 (kW/°C)
UA_e	2.25 (kW/°C)
Solution pump flow rate	0.05 (kg/s)
Effectiveness of solution heat exchanger (ε_{SHX})	0.64
Desorber inlet mass flow rate (water)	1 (kg/s)

showed good agreement as shown in Figure 3. To ensure that the validation process is justified for the integrated system; input parameters for each sub-system are maintained within the suggested range found in the literature. Examples are in maintaining the desorber's inlet temperature for the ACC within the range (50°C-120°C).

3 | SIMULATION INPUT PARAMETERS

The simulation input parameters are given in Tables 2-4. The length of the CPV/T and the mass flow rate were selected such that the outlet temperature would be suitable to run the Stirling engine and the ACC. The rest of the ACC parameters were selected according to the recommendations of the literature.[31]

TABLE 2 CPV/T simulation parameters[36]

Parameter	Value
Concentrator length (L)	12 (m)
Concentrator width (W)	2.5 (m)
Glass cover emissivity (ε_c)	0.87
Receiver tube emissivity (ε_r)	0.92
Glass cover outer diameter (D_g)	90 (mm)
Receiver tube outer diameter (D_o)	50 (mm)
Receiver tube inner diameter (D_i)	40 (mm)
Mirror utilization factor (λ)	0.95
Transitivity of glass cover (τ_c)	0.87
Transitivity (τ_{PV})	0.92
Absorptivity (α_{PV})	0.9
Efficiency at standard conditions (η_0)	0.14
Temperature coefficient (β_{ref})	0.004
Reference temperature (T_{ref})	25 (°C)
Stefan-Boltzmann constant (σ)	5.67×10^{-8} ($W/(m^2.K^4)$)
Specific heat of water with constant pressure (C_p)[37]	4180 (J/kg.K)

4 | RESULTS AND DISCUSSION

For the water vapor to condensate, air must be cooled down below its dew temperature. The integrated system is designed such that the air enters a heat exchanger before each evaporator to reduce its temperature and

TABLE 3 Stirling engine simulation parameters

Specification	Value
Charged gas mass (m_{He})[30]	8×10^{-4}(kg)
Frequency of rotating shaft (F)	20 (Hz)
Gas constant of Helium (R_g)[38]	2077 (J/kg.K)
Specific heat with constant volume for gas (C_v)[30]	3116 (J/kg.K)
Compression specific volume ($v_2 = v_3$)[30]	0.6 (m^3/kg)
Expansion specific volume ($v_1 = v_4$)[30]	1.3 (m^3/kg)
Effectiveness of the regenerator (ε_R)	0.9
Cooler area (A_{sC})[22]	1.2 (m^2)
Heater area (A_{sH})[22]	1.2 (m^2)
Fins effective area (ε_{fin})[39]	1.25 (m^2)
Conventional heat transfer coefficient of water (h_l)[22]	1000 (W/m^2.K)

TABLE 4 Absorption cooling cycle (ACC) simulation parameters

Parameter	Value
UA_a	1.2 (kW/°C)
UA_c	1.2 (kW/°C)
UA_d	1.5 (kW/°C)
UA_e	2 (kW/°C)
Solution pump flow rate	0.05 (kg/s)
Effectiveness of solution heat exchanger (ε_{SHX})	0.64
Desorber inlet mass flow rate (water)	0.5 (kg/s)

exchange heat with the outlet cool air coming out from the evaporator. The minimum temperature that the ambient air can reach before entering the evaporator is its dew point temperature. This heat recovery process can minimize the required sensible cooling by the evaporator. Therefore, it increases the water harvesting rate, especially in dry conditions where the sensible cooling load is very high.

4.1 | The effect of solar radiation

The most influential parameter on power generation and evaporator cooling capacity is solar radiation. Figures 4 and 5 show the effect of solar radiation on the power produced by the Stirling engine and the PV modules and the variation in their efficiencies, along with the COP of the absorption chiller, respectively. An increase in the solar radiation yields an increase in the generated power by both systems since more energy is supplied to them, as shown in Figure 4. At the fixed frequency of 20 Hz for

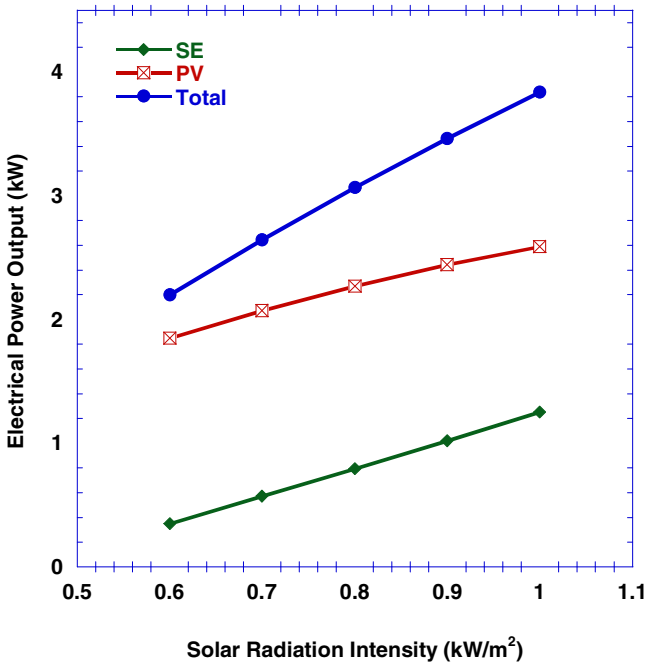

FIGURE 4 Power output from Stirling engine system, PV system and total (kW) as a function of solar radiation intensity (kW/m^2). ($\Phi = 90\%$, $T_{amb} = 30°C$) [Colour figure can be viewed at wileyonlinelibrary.com]

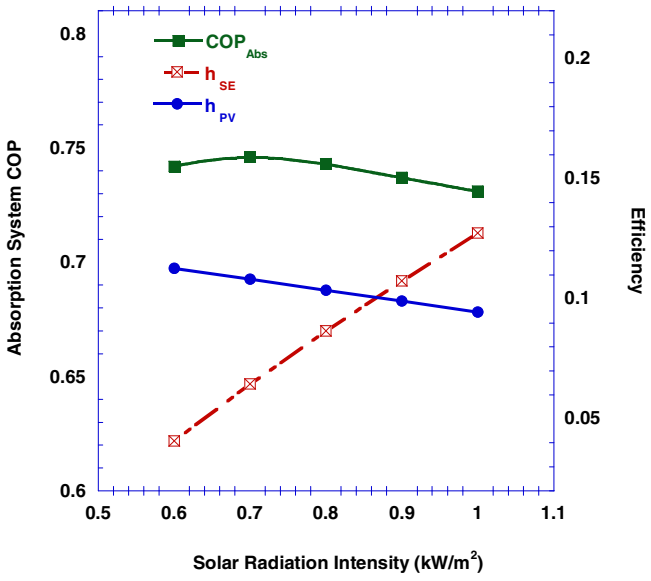

FIGURE 5 Absorption cycle COP, Stirling engine efficiency and PV system efficiency as a function of solar radiation intensity (kW/m^2). ($\Phi = 90\%$, $T_{amb} = 30°C$) [Colour figure can be viewed at wileyonlinelibrary.com]

the Stirling engine, the shaft is rotating at a speed that the low supplied heat at low solar radiation values cannot afford. As the solar radiation increases, the supplied heat is capable of rotating the shaft at that frequency.

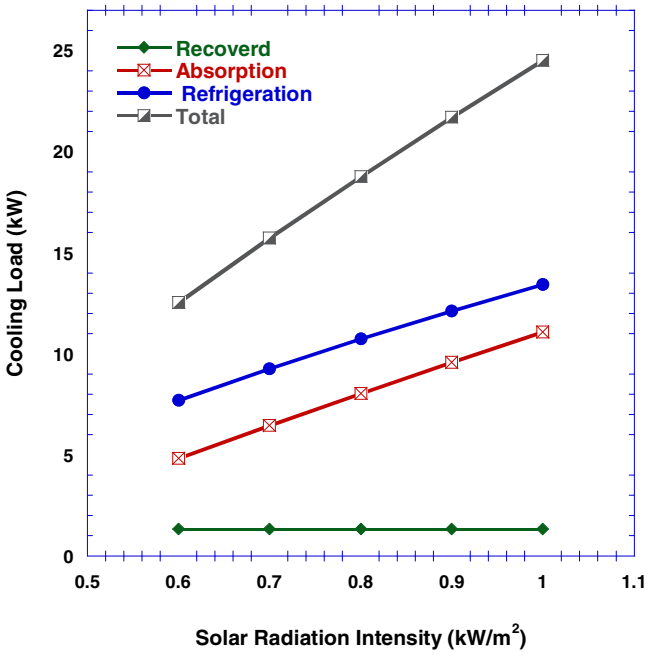

FIGURE 6 Refrigeration, absorption, total and recovered cooling power (kW) as a function of solar radiation intensity (kW/m^2). ($\Phi = 90\%$, $T_{amb} = 30°C$) [Colour figure can be viewed at wileyonlinelibrary.com]

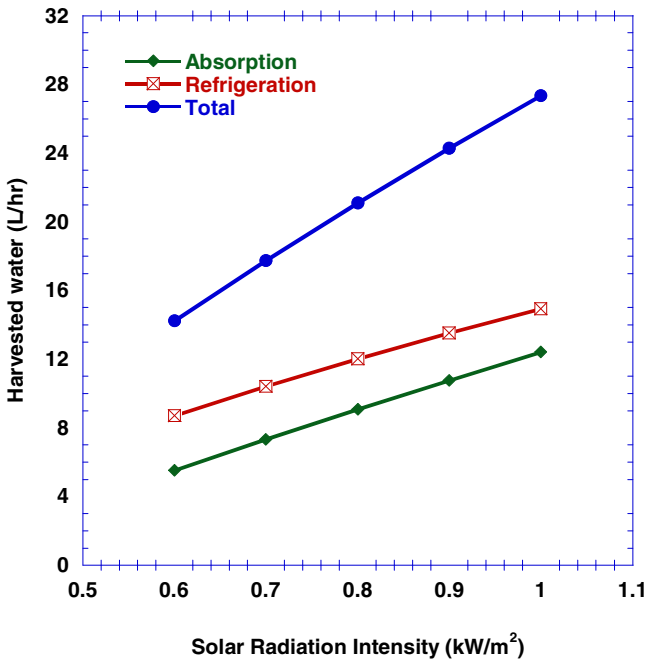

FIGURE 7 Harvested water volume flow rate from refrigeration, absorption and both systems (m^3/h) as a function of solar radiation intensity (kW/m^2). ($\Phi = 90\%$, $T_{amb} = 30°C$, $\dot{m}^*_{air} = 0.7$ kg/s) [Colour figure can be viewed at wileyonlinelibrary.com]

Therefore, the efficiency of the engine increases, as shown in Figure 5.

As for the PV cells, increasing the solar radiation elevates the cells' temperature and decreases their efficiency, see Equation (1). The inlet temperature of the heating stream T_3 varies directly with the solar radiation. Increasing T_3 has different impacts on the desorber's and the evaporator's temperatures. The former increases as T_3 increases, whereas the latter decreases. The absorption chiller COP is expected to increase as the desorber's temperature increases, whereas it is expected to decrease with decreasing the evaporator's temperature. Figure 5 shows that at low values of solar radiation, there is an overall increase in the COP values, but as the solar radiation increases, the duties of the desorber and the evaporator increase as well which reduces the COP slightly.

The effect of solar radiation on the evaporator cooling power is demonstrated in Figure 6. An increase in solar radiation yields a rise in the cooling effect produced by both; the absorption and the refrigeration cycles. The former is a heat-driven cooling system that depends mainly on thermal energy as the driving force; this explains the increase of its cooling power as the solar radiation reaches higher values, whereas the latter depends mainly on the power supplied to the cooling cycle. The heat recovery process is insensitive to the variation of solar radiation as it depends mainly on the relative humidity of ambient air.

The water harvesting rate is directly proportional to the cooling capacity of the cooling cycles, which proved to be a function of solar radiation in Figure 6. Figure 7 shows the hourly rate of the water harvested as a function of the solar radiation. At the solar radiation value of 0.6 kW/m^2 and 90% relative humidity, the system produced 14 L/h approximately, whereas it generated around 28 L/h at a solar radiation value of 1 kW/m^2. The refrigeration cycle is capable of producing 3-4 more liters of harvested water per hour.

4.2 | The effect of ambient temperature

Figure 8 shows the effect of inlet–outlet temperatures as a function of the ambient temperature. It is shown that as the ambient temperature increases, the performance of the refrigeration cycle deteriorates to almost match that of the absorption cycle. This can be explained by Figure 9, which presents the variation of the cooling power of the absorption and the refrigeration and heat recovery process as a function of the ambient temperature. The increase in ambient temperature retards the Stirling engine cooling; since it is cooled by ambient air. Consequently, it reduces the power output of the engine, as expressed in Equations (22) and (23). Moreover, increasing the ambient temperature decreases the

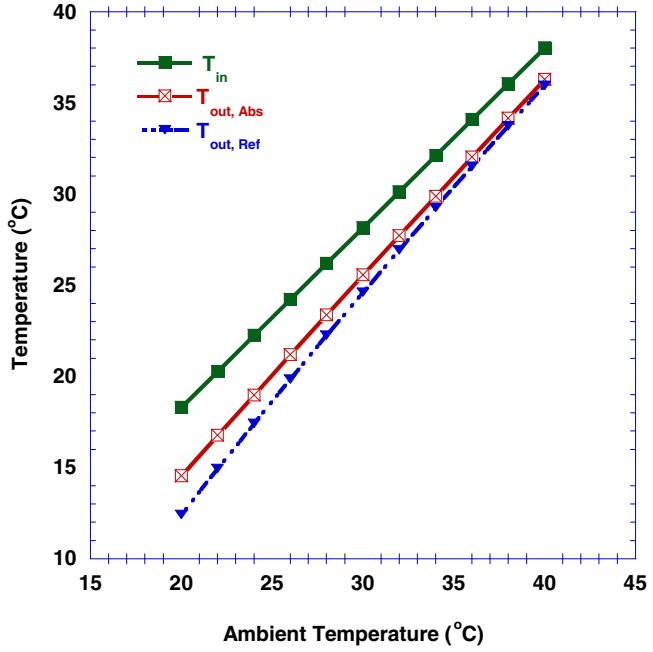

FIGURE 8 Inlet/outlet air temperature to/from the evaporate of both cooling systems as function of ambient temperature (°C). ($\Phi = 90\%$, I = 0.8 kW/m^2, $m^*_{air} = 0.7$ kg/s) [Colour figure can be viewed at wileyonlinelibrary.com]

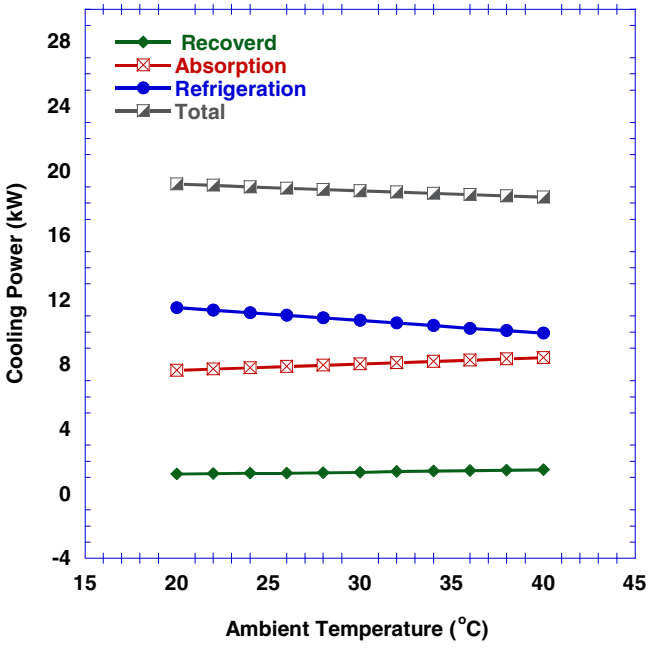

FIGURE 9 Refrigeration, absorption, total and recovered cooling power (kW) as a function of ambient temperature (°C). ($\Phi = 90\%$, I = 0.8 kW/m^2) [Colour figure can be viewed at wileyonlinelibrary.com]

efficiency of the photovoltaic cells according to Equation (2). The cooling capacity of the refrigeration cycle is directly proportional to the power output of both systems.

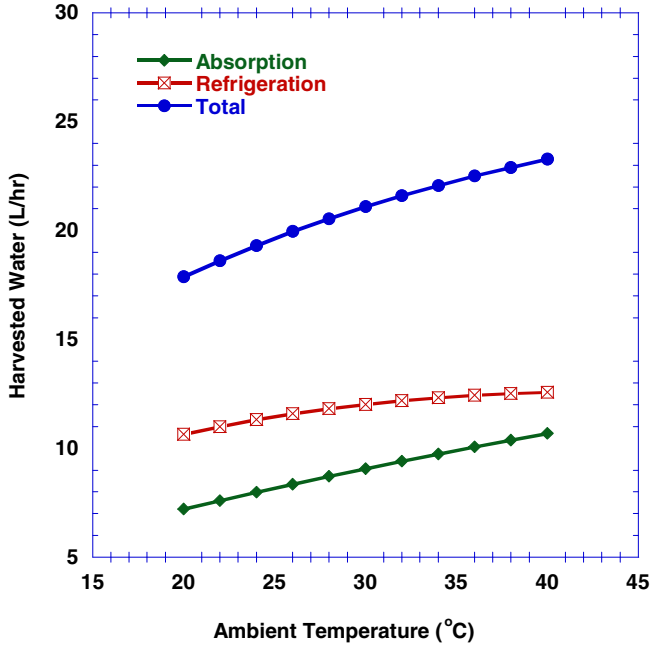

FIGURE 10 Harvested water volume flow rate from refrigeration, absorption and both systems (L/h) as a function of ambient temperature (°C). ($\Phi = 90\%$, I = 0.8 kW/m^2, $m^*_{air} = 0.7$ kg/s) [Colour figure can be viewed at wileyonlinelibrary.com]

Therefore, increasing the ambient temperature reduces the cooling capacity of the refrigeration system. As for the absorption cycle, increasing the ambient temperature raises the heat input into the desorber, which increases the cycle's cooling power. The figure also indicates that the heat recovery process is a weak function of temperature since the relative humidity value is constant.

Ambient air temperature plays a significant role in defining the amount of water content that air can carry before saturating with moisture. As the air temperature increases, the amount of water vapor that can be carried by the air increases as well. Figure 10 shows the effect of ambient temperature on the water harvested (L/h). The system was capable of generating around 18 (L/h) at an ambient temperature of 20°C, whereas it roughly collected 23.5 (L/h) at 40°C.

4.3 | The effect of relative humidity

Relative humidity plays a substantial role in determining the required sensible cooling for the air to start to condensate. Looking at the psychrometric chart, the lower the relative humidity, the higher the sensible cooling to reach the dew point. The heat recovery process aimed to reduce the temperature of the ambient air down to its dew point. When the relative humidity is low, for

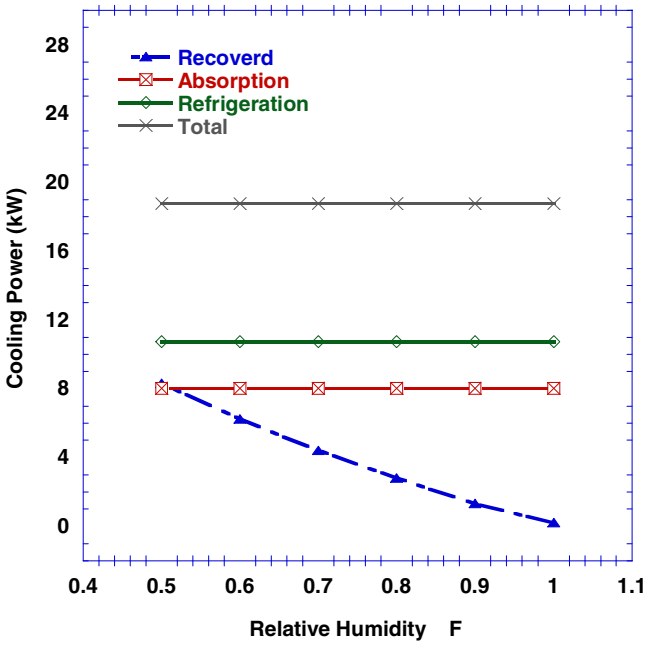

FIGURE 11 Refrigeration, absorption, total and recovered cooling power (kW) as a function of relative humidity. ($T_{amb} = 30°C$, $I = 0.8$ kW/m^2, $m^*_{air} = 0.7$ kg/s [Colour figure can be viewed at wileyonlinelibrary.com]

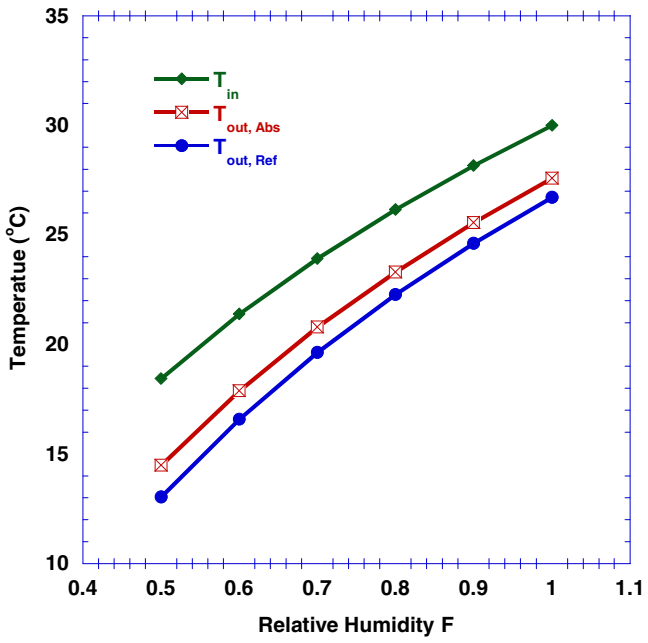

FIGURE 12 Inlet/outlet air temperature to/from the evaporate of both cooling systems as function of relative humidity. ($T_{amb} = 30°C$, $I = 0.8$ kW/m^2, $m^*_{air} = 0.7$ kg/s) [Colour figure can be viewed at wileyonlinelibrary.com]

example, 50%, the dew point is lower than that of high relative humidity values, which increases the duty of the heat-recovery heat exchanger. Figure 11 supports these findings as it shows the variation of the heat transfer during the heat recovery with relative humidity for different ambient temperatures.

The air inlet/outlet temperature variations with relative humidity at a fixed ambient temperature of 30°C are shown in Figure 12. The air inlet temperature decreased from around 30°C to almost 18°C when the relative humidity went from 100% to 50%. To explain this, the system is designed such that the heat recovery heat exchanger reduces the air temperature up to its dew point temperature. At high relative humidity, the dew point is just below the air dry-bulb temperature. Therefore, the air enters the evaporator at a high temperature just below 30°C, whereas it enters the evaporator at temperatures as low as 19°C when the relative humidity is 50%. Since the cooling power is insensitive to the variation in relative humidity, the temperature drop across the evaporator is almost the same for all relative humidity values. Hence, the outlet temperature would follow the same trend as the inlet temperature.

The harvested water (L/h) variation with relative humidity is illustrated in Figure 13. The effect of relative humidity was significantly degraded as the heat recovery was enough to cool the ambient air down to its dew point, where it enters the evaporator with a relative humidity of almost 100%. Nevertheless, increasing the humidity ratio yielded an increase in the total harvested water. One can notice that the saturation line at the psychrometric chart is steeper when the temperature is higher, and it starts to flatten as the temperature decreases. In other words, the hot air which carries more water can produce more water than that colder air as it cools down. The total harvested water was just below 18 (L/h) at a relative humidity value of 50%, and it gradually increased to reach just over 21 (L/h) at a relative humidity of 100%.

4.4 | The effect of air mass flow rate

The harvested water variation as a function of the air mass flow rate is presented in Figure 14 for different solar radiation values. To start with, according to Equation (33), the water harvesting rate is a function of the specific humidity ratio difference between inlet and outlet conditions, which is a function of the air mass flow rate. At low values of air mass flow rate, the air is cooled to lower temperatures, which increases the specific humidity ratio difference. On the other hand, at high values of air mass flow rate, the evaporator has to deal with more air mass, and the outlet-specific humidity ratio at the outlet would be closer to that of the air at the inlet. At some point in between, there an optimum mass flow

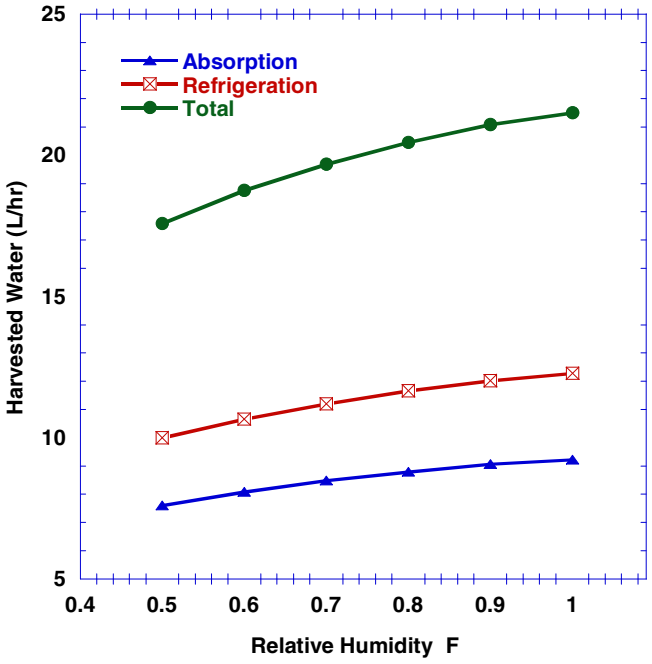

FIGURE 13 Harvested water volume flow rate from refrigeration, absorption and both systems (L/h) as function of relative humidity ($T_{amb} = 30°C$, $I = 0.8$ kW/m^2, $m^*_{air} = 0.7$ kg/s) [Colour figure can be viewed at wileyonlinelibrary.com]

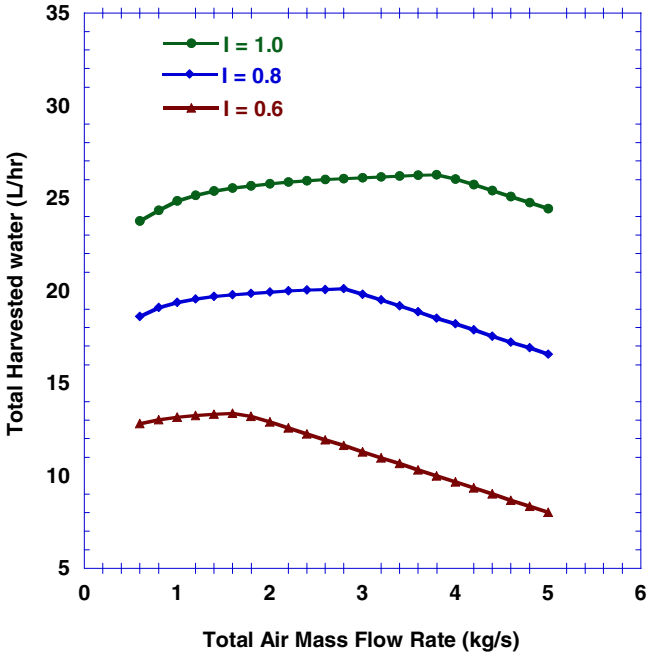

FIGURE 14 Total harvested water volume flow rate (L/h) as a function of total air mass flow rate (kg/s) for different solar radiation intensity (kW/m^2). ($\Phi = 70\%$, $T_{amb} = 30°C$) [Colour figure can be viewed at wileyonlinelibrary.com]

rate of air that would generate the maximum amount of water. The results show that as the solar radiation increases, the system can deal with more air mass, thus more water is produced. At solar radiation values of 0.6, 0.8, and 1 (kW/m^2), the maximum water production was generated at air mass flow rate values of 1.6, 2.8, and 3.8 (kg/s), and the corresponded water production were 13.37, 20.12, and 26.28 (L/h), respectively.

4.5 | Sizing approach: case study

The following calculations provide a rough estimation for the size based on daily water needs for building in Jordan. The daily water consumption is 164 L, and the corresponding cooling effect needed to provide this amount is approximately estimated as:

$$Q_{condensate} = (\dot{m}_{water})(h_{fg}) \tag{35}$$

where $\dot{m}_{water}$ is the daily water consumption and h_{fg} is the enthalpy of evaporation of water.

The cooling effect duty is assumed to be shared by the absorption and the refrigeration cooling cycles, therefore, half of the required cooling effect is produced by the ACC and estimated as:

$$Q_{e,ACC} = (0.5)(Q_{condensate}) \tag{36}$$

Knowing that the average (COP_{ACC}) of the ACC is around 0.7, the required heat input for the desorber (Q_d) can be calculated using the following equation:

$$Q_d = \frac{Q_{e,ACC}}{COP_{ACC}} \tag{37}$$

As for the refrigeration cooling cycle, the cooling effect duty is estimated as:

$$Q_{e,VCRC} = (0.5)(Q_{condensate}) \tag{38}$$

Taking into consideration that the (COP_{VCRC}) of a refrigeration cooling cycle is approximately around 3, the required work input for the compressor can be calculated using the following equation:

$$(P_{tot}) = \frac{Q_{e,VCRC}}{(COP_{VCRC})} \tag{39}$$

According to the simulation provided in this research, the photovoltaic cells were capable of producing electrical power twice as much as the Stirling engine. This can be explained by the limitation of the hot stream temperature that feeds the hot cylinder of the Stirling engine to be less than 110°C since the single effect ACC and the

photovoltaic cells cannot deal with higher temperatures. Based on that, two-thirds of the compressor work should be provided by the photovoltaic cells, whereas the Stirling engine would provide the remaining one-third.

$$P_{PV} = (2/3)(W_{comp}) \tag{40}$$

$$P_{SE} = (1/3)(W_{comp}) \tag{41}$$

The energy balance for the water loop across the CPV/T, the Stirling engine, and the ACC is calculated as:

$$Q_{in} - Q_{loss} - Q_H - Q_d - \mathrm{P_{PV}} = 0 \tag{42}$$

where Q_{in} is the heat input, Q_H is the heat input into the hot cylinder of the Stirling engine, Q_d is the heat input into the desorber of the ACC. Q_{loss} represents the total heat loss in the concentrator due to convection, radiation, and optical losses. The parabolic concentrator has a typical efficiency of around 75%, and Q_{loss} is estimated as:

$$Q_{loss} = \eta_{PTC} Q_{in} \tag{43}$$

$\mathrm{P_{PV}}$ represents the power output of the photovoltaic cells, and is calculated as:

$$\mathrm{P_{PV}} = Q_{in}\eta_{\mathrm{PV}}$$

The efficiency of the concentrated photovoltaic modules (η_{PV}) is around 10%, whereas the Stirling engine efficiency (η_{SE}) within the specified temperature range ($\mathrm{T_H}$ around 100°C and $\mathrm{T_L}$ around 40°C) is around 15%. The required input energy for the Stirling engine (Q_H) is calculated as:

$$Q_H = \frac{P_{SE}}{\eta_{SE}} \tag{44}$$

Once Q_{in} is estimated, the area of the concentrator can be identified. The average daily solar irradiance Q_{solar} in Jordan is 6 kWh/m^2.[40] The concentrator area can be estimated as:

$$A_c = \frac{Q_{in}}{Q_{solar}} \tag{45}$$

4.6 | Sample of calculations

According to the simulation input parameters in Table 5, the concentrator area was set to be 30 m^2. Figure 7 shows that at solar radiation 1 kW/m^2, the system produced 28 L/h. For 6 hours of working time (average daily solar irradiance Q_{solar} in Jordan is 6 kWh/m^2), the cumulative harvested water is 168 L. The estimated concentrator area (30.38 m^2) is very close to the exact area of the concentrator (30 m^2). The relative error between the estimated solution and the exact solution is computed as:

$$Error\% = \frac{(A_{c,estimated} - A_{c,actual})}{A_{c,actual}} \tag{46}$$

The error is within 1.3%.

5 | COMPARISON WITH PREVIOUS STUDIES AND OTHER TECHNOLOGIES

The current results were compared to existing work in the literature in terms of the energy intensity per liter. The system's energy intensity, or the amount of energy consumed per liter of produced water, is just as significant as the amount of water produced. It comprises the electrical energy consumption of electrical components (such as compressors, fans) and the thermal energy in humidification–dehumidification solar distillation system. Zolfagharkhani et al[41] have reported an energy intensity between 250 and 450 Wh/L of electricity, whereas the proposed system in this research has an energy intensity between 225 and 315 Wh/L

TABLE 5 Sample of calculations for the sizing approach

Sample of calculation for 168 L/d water demand			
Variable	**Value**	**Variable**	**Value**
Total cooling load (Q_e)	411 600 kJ	Photovoltaic work ($\mathrm{P_{PV}}$)	45 733.3 kJ
Absorption cooling load ($Q_{e,ACC}$)	205 800 kJ	Stirling engine work (P_{SE})	22 866.7 kJ
Refrigeration cooling load ($Q_{e,VCRC}$)	205 800 kJ	Input energy for the Stirling (Q_H)	152 444.4 kJ
Desorber's heat input (Q_d)	294 000 kJ	Required thermal energy (Q_{in})	656 237 kJ
Work input (P_{tot})	68 600 kJ	Concentrator area (A_c)	30.38 m^2

approximately. As for the thermal energy, the solar humidification–dehumidification distillation (HDD) systems have an energy intensity of about 700 Wh/L.[42,43] Although generating fresh water via an ACC has a higher thermal energy per liter demand, around 1000-2000 Wh/L, it can produce both freshwater and cooling effect, unlike the HDD systems which produce freshwater only. Moreover, the HDD systems are justified only when water resources do exist, whereas the current system can work in the absence of any water resources. The integration of this system makes it possible to have multiple outputs; freshwater, electrical power, cooling effect, and heating.

6 | LIMITATION OF THE PROPOSED SYSTEM

The proposed system is limited in terms of the amount of harvested water. The concentrator area plays a significant role in determining the daily rate of water as it defines the cooling capacity of the system. As the concentrator area increases, the temperature of the working fluid increases as well. Increasing the concentrator area is allowed as long as the temperature of the working fluid does not exceed the recommended working temperatures for the components; examples are the photovoltaic cells' temperature and the desorber's inlet temperature. Therefore, the proposed system is suitable for small-scale applications where water demand is up to 180 L/day.

7 | CONCLUSION

One of humanity's most daunting problems in the future would be water shortages. The global water demand is growing dramatically. Interestingly, about one-tenth of all the water on the earth lies in the atmosphere. Air-water harvesting technologies (AWH) can be used in remote areas, where annual precipitation is limited or no rivers, lakes, or other resources are available. This paper proposes a new atmospheric water harvesting system, which consists of a concentrated photovoltaic thermal (CPVT), a Stirling engine (SE), an ACC, and a VCRC. The CPV/T was employed for the cogeneration of heat and electricity, where the heat was utilized to drive the Stirling engine as well as the ACC. The electrical power output of the CPV/T and the Stirling engine was used to drive the vapor compression cycle. The cooling power of the ACC and the VCRC was responsible for the dehumidification process and water production. Moreover, a heat recovery heat exchanger was employed to precool the supply air, thus enhancing the condensation process. The mathematical model was solved numerically using EES software, where its performance was investigated under different ambient and operating conditions.

The simulation results show that the water production rate is enhanced monotonically by increasing the solar radiation, the ambient temperature, and the relative humidity. The hourly harvested water was ranging from 14 (for cold and dry conditions) to 28 L/h (for hot and dry conditions). However, the supplied air mass flow rate had a non-monotonic effect on freshwater production. At solar radiation values of 0.6, 0.8, and 1 (kW/m^2), the maximum water production was generated at air mass flow rate values of 1.6, 2.8, and 3.8 (kg/s), respectively. The system can produce up to 30 L/h in conditions where the solar radiation is 1 kW/m^2, the ambient temperature is 40°C, and the relative humidity is 100%. The results also demonstrate that precooling the ambient air can enhance water production in dry conditions. The system's energy intensity is found to be between 225 and 315 Wh/L approximately. For future work, it is suggested to investigate the effect of cooling the Stirling engine by the outlet cold air stream thus enhancing its efficiency and increasing the freshwater harvesting rate. Moreover, it is recommended to build a prototype to validate the results experimentally.

NOMENCLATURE

A_c	Area of the concentrator (m^2)
A_g	Glass cover outer area (m^2)
A_{pv}	Photovoltaic module area (m^2)
A_r	Receiver tube outer area (m^2)
$A_{s,H}$	Area of Stirling engine heater (m^2)
$A_{s,L}$	Area of Stirling engine cooler (m^2)
C_p	Specific heat of water at constant pressure (kJ/kg.°C)
C_v	Specific heat of Helium gas at constant volume (kJ/kg.°C)
D_i	Copper tube internal diameter (mm)
D_o	Copper tube outside diameter (mm)
D_g	Glass layer outside diameter (mm)
F	Rotating frequency of Stirling engine shaft (Hz)
FR	Heat removal factor
h	Enthalpy of substance (kJ/kg)
$h_{r\,g-pv}$	Heat transfer coefficient due to radiation between the photovoltaic module and the glass layer ($W/m^2.°C$)
$h_{r\,a-g}$	Heat transfer coefficient due to radiation between the glass layer and the ambient ($W/m^2.°C$)
$h_{f,in}$	Heat transfer coefficient due to convection in the copper tube ($W/m^2.°C$)

I	Solar radiation intensity (kW/m^2)
K_a	Air thermal conductivity (W/m.°C)
K_H	Heat transfer ability at the hot end (kW/°C)
K_L	Heat transfer ability at the cold end (kW/°C)
K_w	Water thermal conductivity (W/m.K)
$\dot{m}$	The mass flow rate of water (kg/s)
m_{He}	Mass of charged gas (kg)
Nu	Nusselt number
P_{PV}	The electrical power produced by the photovoltaic cells (kW)
P_{SE}	The electrical power produced by the Stirling engine (kW)
P_{tot}	Total electrical power generated by the system (kW)
Q	Rate of heat transfer (kW)
Re	Reynold number
R_g	Gas constant (kJ/kg.°C)
T_a	Ambient temperature (°C)
T_g	The temperature of the glass cover (°C)
T_H	Heat absorbing temperature of charged gas (°C)
T_L	Heat rejection temperature of charged gas (°C)
T_{sky}	Sky temperature (°C)
UA	Overall heat transfer coefficient (kW/°C)
V_w	Wind speed (m/s)
X	Vapor quality

GREEK SYMBOLS

β	Thermal expansion coefficient (1/K)
ϵ_g	Glass emissivity
ε_{fin}	Fins effectiveness
$\varepsilon_{hr,HX}$	Effectiveness of heat recovery heat exchanger
ε_R	Effectiveness of Stirling engine regenerator
ε_{SHX}	Effectiveness of solution heat exchanger
γ	Mirror utilization factor
η_0	The efficiency of the photovoltaic cells at standard conditions
η_{PV}	The actual efficiency of photovoltaic cells
η_{SE}	Stirling engine efficiency
ρ	Water density (kg/m^3)
σ	Stefan-Boltzmann constant [kW/m^2.^{0}C]
v	Specific volume (m^3/kg)
τ_g	Glass transmissivity
μ	Dynamic viscosity (Pa· s)

SUBSCRIPTS

a	Ambient
e	Evaporator
H	Hot end
i	Inlet
L	Cold end
o	Outlet

ACKNOWLEDGEMENT

This research did not receive any specific grant from any funding agency in the public, commercial, or not-for-profit sectors.

ORCID

Ibrahim Al Keyyam https://orcid.org/0000-0002-0448-8096

Ashraf Keewan https://orcid.org/0000-0003-3218-8063

REFERENCES

1. Conn AW, Barker GA. Fresh water drowning and near-drowning-an update. *Can. Anaesth. Soc. J.* 1984;31(3):38–44. https://doi.org/10.1007/BF03007034.
2. UNESCO. The United Nations World Water Development Report 2018: Nature-Based Solutions for Water; 2018.
3. Milani D, Qadir A, Vassallo A, Chiesa M, Abbas A. Experimentally validated model for atmospheric water generation using a solar assisted desiccant dehumidification system. *Energy Build.* 2014;77:236–246. https://doi.org/10.1016/j.enbuild.2014.03.041.
4. Dalai P, Nanda P, Mund C, Mishra D, Gupta A. An experimental study on water harvesting from a modified window air-conditioner. *Energy Procedia*. 2016;109:253-260. https://doi.org/10.1016/j.egypro.2017.03.058.
5. Larson R, Mountain I. Air conditioning and water-harvesting. 2015;1(19).
6. Al-Farayedhi AA, Ibrahim NI, Gandhidasan P. Condensate as a water source from vapor compression systems in hot and humid regions. *Desalination*. 2014;349:60-67. https://doi.org/10.1016/j.desal.2014.05.002.
7. Ibrahim NI, Al-Sulaiman FA, Saidur R. Performance assessment of water production from solar cooling system in humid climate. *Energy Convers Manage*. 2016;127:647-655. https://doi.org/10.1016/j.enconman.2016.09.056.
8. Salek F, Moghaddam AN, Naserian MM. Thermodynamic analysis and improvement of a novel solar driven atmospheric water generator. *Energy Convers. Manage*. 2018;161:104-111. https://doi.org/10.1016/j.enconman.2018.01.066.
9. Magrini A, Cattani L, Cartesegna M, Magnani L. Integrated systems for air conditioning and production of drinking water-preliminary considerations. *Energy Procedia*. 2015;75:1659-1665. https://doi.org/10.1016/j.egypro.2015.07.406.
10. Joshi VP, Joshi VS, Kothari HA, Mahajan MD, Chaudhari MB, Sant KD. Experimental investigations on a portable fresh water generator using a thermoelectric cooler. *Energy Procedia*. 2017;109:161-166. https://doi.org/10.1016/j.egypro.2017.03.085.
11. Milani D, Abbas A, Vassallo A, Chiesa M, Al Bakri D. Evaluation of using thermoelectric coolers in a dehumidification system to generate freshwater from ambient air. *Chem Eng Sci.* 2011;66(12):2491-2501. https://doi.org/10.1016/j.ces.2011.02.018.
12. Pontious K, Weidner B, Guerin N, Dates A, Pierrakos O, Altaii K. Design of an atmospheric water generator: harvesting water out of thin air. Paper presented at: 2016 IEEE Systems and Information Engineering Design Symposium (SIEDS);

April 29-29, 2016; Charlottesville, VA:6-11. https://doi.org/10.1109/SIEDS.2016.7489327.
13. Atta RM. Solar water condensation using thermoelectric coolers. *Int. J. Adv. Eng. Res. Dev*. 2017;4(09):142-145. https://doi.org/10.21090/ijaerd.96616.
14. Eslami M, Tajeddini F, Etaati N. Thermal analysis and optimization of a system for water harvesting from humid air using thermoelectric coolers. *Energy Convers. Manage*. 2018;174:417-429. https://doi.org/10.1016/j.enconman.2018.08.045.
15. Muñoz-García MA, Moreda GP, Raga-Arroyo MP, Marín-González O. Water harvesting for young trees using Peltier modules powered by photovoltaic solar energy. *Comput Electron Agric*. 2013;93:60-67. https://doi.org/10.1016/j.compag.2013.01.014.
16. Giwa A, Fath H, Hasan SW. Humidification-dehumidification desalination process driven by photovoltaic thermal energy recovery (PV-HDH) for small-scale sustainable water and power production. *Desalination*. 2016;377:163-171. https://doi.org/10.1016/j.desal.2015.09.018.
17. Mahmoud A, Fath H, Ahmed M. Enhancing the performance of a solar driven hybrid solar still/humidification-dehumidification desalination system integrated with solar concentrator and photovoltaic panels. *Desalination*. 2018;430:165-179. https://doi.org/10.1016/j.desal.2017.12.052.
18. Jabari F, Nazari-heris M, Mohammadi-ivatloo B, Asadi S, Abapour M. A solar dish Stirling engine combined humidification-dehumidification desalination cycle for cleaner production of cool, pure water, and power in hot and humid regions. *Sustainable Energy Technol. Assess*. 2020;37:100642. https://doi.org/10.1016/j.seta.2020.100642.
19. Al-Nimr MA, Al-Ammari WA. A novel hybrid and interactive solar system consists of Stirling engine/vacuum evaporator/thermoelectric cooler for electricity generation and water distillation. *Renewable Energy*. 2020;153:1053-1066. https://doi.org/10.1016/j.renene.2020.02.072.
20. Elashmawy M, Alshammari F. Atmospheric water harvesting from low humid regions using tubular solar still powered by a parabolic concentrator system. *J Clean Prod*. 2020;256:120329. https://doi.org/10.1016/j.jclepro.2020.120329.
21. Wang W, Xie S, Pan Q, Dai Y, Wang R, Ge T. Air-cooled adsorption-based device for harvesting water from island air. *Renewable and Sustainable Energy Reviews*. 2021;141:110802. http://dx.doi.org/10.1016/j.rser.2021.110802.
22. Al-Nimr M, Kiwan S, Keewan A. A novel approach to improve the performance of solar-driven Stirling engine using solar-driven ejector cooling cycle. *Int. J. Energy Res*. 2020;44:1–21. https://doi.org/10.1002/er.5657.
23. Sharadga H, Dawahdeh A, Al-Nimr MA. A hybrid PV/T and Kalina cycle for power generation. *Int J Energy Res*. 2018;42(15):4817-4829. https://doi.org/10.1002/er.4237.
24. Al-Nimr MA, Kiwan S, Sharadga H. Simulation of a novel hybrid solar photovoltaic / wind system to maintain the cell surface temperature and to generate electricity. *Int. J. Energy Res*. 2018;42:985-998. https://doi.org/10.1002/er.3885.
25. Kalogirou SA. *Solar Energy Engineering Processes and Systems*. United States: Academic Press; 2014.
26. Incropera ASLF, Dewitt D, Bergman T. *Principles of Heat and Mass Transfer*. 7th intern ed. United States: Wiley; 2013.
27. Nasrin R, Hasanuzzaman M, Rahim NA. Effect of high irradiation and cooling on power, energy and performance of a PVT system. *RenewableEnergy*. 2018;116:552-569. https://doi.org/10.1016/j.renene.2017.10.004.
28. Liu W, Liu ZC, Ma L. Application of a multi-field synergy principle in the performance evaluation of convective heat transfer enhancement in a tube. *Chin Sci Bull*. 2012;57(13):1600-1607. https://doi.org/10.1007/s11434-012-5062-x.
29. Qiu Y, Li MJ, Wang WQ, Du BC, Wang K. An experimental study on the heat transfer performance of a prototype molten-salt rod baffle heat exchanger for concentrated solar power. *Energy*. 2018;156:63–72. https://doi.org/10.1016/j.energy.2018.05.040.
30. Lai X, Yu M, Long R, Liu Z, Liu W. Dynamic performance analysis and optimization of dish solar Stirling engine based on a modified theoretical model. *Energy*. 2019;183:573-583. https://doi.org/10.1016/j.energy.2019.06.131.
31. Herold S, Klein KE. *Absorption Chillers and Heat Pumps*. 2nd ed.; United States: CRC Press; 1996.
32. Darwish Ahmad A, Abubaker AM, Najjar YSH, Manaserh YMA. Power boosting of a combined cycle power plant in Jordan: an integration of hybrid inlet cooling & solar systems. *Energy Convers. Manage*. 2020;214:112894. https://doi.org/10.1016/j.enconman.2020.112894.
33. Ge TS, Dai YJ, Wang RZ. Review on solar powered rotary desiccant wheel cooling system. *Renewable Sustainable Energy Rev*. 2014;39:476–497. https://doi.org/10.1016/j.rser.2014.07.121.
34. Cengel YA, Boles MA. *Thermodynamics: an Engineering Approach*. 8th ed.; United States: McGraw Hill; 2015.
35. Mardiana-Idayu A, Riffat SB. Review on heat recovery technologies for building applications. *Renewable Sustainable Energy Rev*. 2012;16:1241–1255. https://doi.org/10.1016/j.rser.2011.09.026.
36. Al-Nimr MA, Mugdadi B. A hybrid absorption/thermo-electric cooling system driven by a concentrated photovoltaic/thermal unit. *Sustainable Energy Technol. Assess*. 2020;40:100769. https://doi.org/10.1016/j.seta.2020.100769.
37. Najjar YSH, Manaserh YMA. Aligning combined cycle power plant performance with field measurements. *Arab J Sci Eng*. 2019;44(2):1657-1669. https://doi.org/10.1007/s13369-018-3615-2.
38. In S, Jeong S, Kim H. Investigation on liquid helium pressurization process using a heater in a liquid propellant rocket. *Cryogenics*. 2004;44(6–8):467-474. https://doi.org/10.1016/j.cryogenics.2004.02.010.
39. Micheli L, Reddy KS, Mallick TK. Thermal effectiveness and mass usage of horizontal micro-fins under natural convection. *Appl Therm Eng*. 2016;97:39-47. https://doi.org/10.1016/j.applthermaleng.2015.09.042.
40. Alrwashdeh SS, Alsaraireh FM, Saraireh MA. Solar radiation map of Jordan governorates. *Int. J. Eng. Technol*. 2018;7(3):1664. https://doi.org/10.14419/ijet.v7i3.15557.
41. Zolfagharkhani S, Zamen M, Shahmardan MM. Thermodynamic analysis and evaluation of a gas compression

refrigeration cycle for fresh water production from atmospheric air. *Energy Convers. Manage*. 2018;170:97-107. https://doi.org/10.1016/j.enconman.2018.05.016.

42. Soufari SM, Zamen M, Amidpour M. Experimental validation of an optimized solar humidification-dehumidification desalination unit. *Desalin Water Treat*. 2009;6(1–3):244-251. https://doi.org/10.5004/dwt.2009.494.
43. Zamen M, Soufari SM, Vahdat SA, et al. Experimental investigation of a two-stage solar humidification-dehumidification desalination process. *Desalination*. 2014;332(1):1-6. https://doi.org/10.1016/j.desal.2013.10.018.

How to cite this article: Al Keyyam I, Al-Nimr M, Khashan S, Keewan A. A new solar atmospheric water harvesting integrated system using CPV/T – Stirling engine – Absorption cooling cycle and vapor compression refrigeration cycle. *Int J Energy Res*. 2021;1–18. https://doi.org/10.1002/er.6888